Toward Wideband Steerable Acoustic Metasurfaces with Arrays of Active Electroacoustic Resonators

This manuscript has been accepted for publication in the Journal of Applied Physics on January 14, 2018.

Hervé Lissek,[1, a)] Etienne Rivet,[1] Thomas Laurence,[1] and Romain Fleury[2]
[1)] *Ecole Polytechnique Fédérale de Lausanne, Laboratory of Signal Processing 2, EPFL STI IEL LTS2, Station 11, CH-1015 Lausanne, Switzerland.*
[2)] *Ecole Polytechnique Fédérale de Lausanne, Laboratory of Wave Engineering, EPFL STI IEL LWE, Station 11, CH-1015 Lausanne, Switzerland.*

(Dated: 14 January 2018)

We introduce an active concept for achieving acoustic metasurfaces with steerable reflection properties, effective over a wide frequency band. The proposed active acoustic metasurface consists in a surface array of subwavelength loudspeakers diaphragms, each with programmable individual active acoustic impedances allowing for local control over the different reflection phases over the metasurface. The active control framework used for controlling the reflection phase over the metasurface is derived from the Active Electroacoustic Resonator concept. Each unit-cell simply consists of a current-driven electrodynamic loudspeaker in a closed box, whose acoustic impedance at the diaphragm is judiciously adjusted by connecting an active electrical control circuit. The control is known to achieve a wide variety of acoustic impedances on a single loudspeaker diaphragm used as an acoustic resonator, with the possibility to shift its resonance frequency by more than one octave. The paper presents a methodology for designing such active metasurface elements. An experimental validation of the achieved individual reflection coefficients is presented, and full wave simulations present a few examples of achievable reflection properties, with a focus on the bandwidth of operation of the proposed control concept.

PACS numbers: 43.20.El, 43.20.Tb, 43.38.Hz
Keywords: Active acoustic metasurface, adjustable reflectarray, electroacoustic resonators, active acoustic impedance control

I. INTRODUCTION

Acoustic Metasurfaces (AMS) designate surface arrangements of subwavelength unit-cells that are engineered so as to artificially reshape wavefronts out of an impinging sound pressure field, owing to a prescribed variation of local acoustic properties. They are essentially envisaged as interfaces with exogenous propagating media, whereas Acoustic Metamaterials (AMM) rather refer to wave manipulations within the artificial medium[1] (although connection with an external medium are also envisaged in Leaky-Wave Antenna applications[2,3]). Metasurfaces can then be designed to reflect wavefronts in an anomalous manner ("reflectarray"), with potential application to acoustic cloaking[4,5], or for sound transmission manipulation ("transmit-array")[6] with application to acoustic lensing. They can also be applied to sound chanelling[7,8] and sound absorption[9].

The manipulation of acoustic wavefronts in a reflectarray is achieved by adequately distributing the phase of the reflection coefficient over the metasurface. Several concepts have been investigated to artificially control the reflection phase of a unit-cell, while remaining small with respect to the wavelength. Spiral acoustic unit-cells have been proposed, allowing lengthening the acoustic path through a labyrinthine-type channel inside the unit-cell[5,10]. Helmholtz resonators are also obvious solutions, since their resonance frequency can be tuned by tailoring their cavity and neck dimensions. By selecting gradually varying Helmholtz resonances, the reflection coefficient phase can be adjusted to a target distribution[11,12]. Alternatively, membrane-type acoustic metasurfaces have been proposed achieving acoustic impedance gratings either by adequate spacing between membranes[13], or by adapting the membrane thicknesses[4]. Such passive AMS concepts have been thoroughly investigated to derive design guidelines and assess their performance mostly at a computational stage. Some studies have reported practical realization of acoustic metasurfaces. Besides the application to cloaking[11], a recent paper of Jimenez et al[12] reports the design of an acoustic metasurface based on stacked coupled Helmholtz resonators, that allows achieving controllable sound diffusion for use in room acoustics. Meanwhile, passive AMS suffer from drastic limitations: they are inherently narrow-band at a prescribed frequency due to their resonant behaviour[14], and they cannot be reconfigured in real-time. Since the properties of the AMS are fixed by design (geometry and material properties), it makes passive AMS concepts irrelevant to most practical acoustic problems, with respect to bandwidth and reconfigurability. This motivated the development of a new class of AMS implementing active unit-cells concepts, such as piezoelectric membranes with dedicated feedback-control units, allowing for real

[a)] Electronic mail: herve.lissek@epfl.ch

time reconfiguration of a metamaterial slab to achieve prescribed lensing properties[15]. Alternatively, an active acoustic metasurface (AAMS) concept implementing a spatial arrangement of unit-cells, composed of a membrane with an attached magnetic mass actuated by an electromagnetic transducer, has been proposed to allow reflection reconfigurability[16]. Although the literature on active acoustic metasurfaces mainly addresses reconfigurability aspects, the possibility to extend the control bandwidth has been less investigated, due to a lack of stable broadband active control concepts.

The concept of Active Electroacoustic Resonators (AER), firstly developed for achieving broadband sound absorption in the low-frequency range[17–20], may represent an interesting solution to this problem by providing an adjustable and/or broadband unit-cell for AAMS applications[21–23]. The control scheme at work in such AER assigns a target acoustic impedance to the diaphragm of the current-driven loudspeaker, through a sensor-/shunt-based impedance control[19]. With this techniques, a same Electroacoustic Resonator can be dynamically tuned to a wide range of resonance frequencies or quality factors, through a somehow simple control law. Since the manipulation of wavefronts at the heart of the AMS concept requires assigning prescribed acoustic impedances to the unit-cells, and since it can be achieved on a broadband manner with AER, it is expected to overcome the usual limitations (eg. bandwidth) of the passive AMS concepts reported so far in the literature.

In this paper, the concept of an AAMS composed of a 2D arrangement of subwavelength AER is introduced aiming at achieving broadband and steerable (reconfigurable) anomalous reflection. The first section reminds the general properties of the proposed AMS framework, with a focus on the control parameters over the metasurface allowing the reflection direction for a given incident plane wave. In the second section, the AER concept is presented. Then a methodology is introduced that sets unit-cells controllers in order to achieve the prescribed reflection properties, followed by an experimental validation of the achieved acoustic properties. Finally, a few examples of reflectarray settings will be discussed, based on simulations with a commercial finite-elements software (COMSOL Multiphysics).

II. MEMBRANE-TYPE ACOUSTIC METASURFACE

A. Description of the proposed Acoustic Metasurface

The proposed AMS consists of subwavelength unit-cells spatially arranged over a planar lattice (over the "horizontal" plane xOy), aiming at controlling the reflected wavefronts for any arbitrary incident plane waves. The subwavelength condition imposes that the lattice constant $d_d < \frac{\lambda_{max}}{10}$, where $\lambda_{max} = \frac{c_0}{f_{max}}$ is the wavelength corresponding to the upper working frequency f_{max}, with $c_0 = 343$ m.s^{-1} the sound celerity in the air. We denote the reflection coefficient by $\Gamma(x,y)$ at each point (x,y) over the AMS, and its phase by $\psi(x,y)$. Any incident [respectively reflected] plane wave will be characterized in the following by its wave-vector $\vec{k}_i$ $(cos(\phi_i),sin(\phi_i),cos(\theta_i))$ [respectively $\vec{k}_r$ $(cos(\phi_r),sin(\phi_r),cos(\theta_r))$], where ϕ_i [respectively ϕ_r] is the azimuth over the AMS plane and θ_i [respectively θ_r] the elevation of the incident [respectively reflected] plane wave vector.

According to Ref.[4], in order to prescribe the wave-vector k_r of the reflected wave for a given wave-vector k_i of the incident wave, at given frequency f, the reflection phase gradient $\vec{\nabla}\psi(x,y)$ should satisfy:

$$\frac{\partial\psi}{\partial x} = -\frac{2\pi f}{c_0}\left(sin\theta_r cos\phi_r + sin\theta_i cos\phi_i\right), \tag{1a}$$

$$\frac{\partial\psi}{\partial y} = -\frac{2\pi f}{c_0}\left(sin\theta_r sin\phi_r + sin\theta_i sin\phi_i\right). \tag{1b}$$

These conditions can also be formulated for a discrete arrangement of subwavelength reflectors. We now consider the 2D arrangement of small identical circular pistons of radius r_d over the AMS plane as illustrated in Figure 1. In this configuration, we consider the regular lattice over directions x and y with a same lattice constant $d_d = 2r_d$, so that the center of each disk is located at (x_0^m,y_0^n) with $x_0^m = (m-1)\,d_d + x_0$ and $y_0^n = (n-1)\,d_d + y_0$, and (x_0,y_0) the position of the first cell of the lattice. The subwavelength conditions then imposes that $r_d < \frac{c_0}{20\,f_{max}}$, which corresponds to a maximum disk radius of about 34 mm at 500 Hz.

Each disk, denoted by the couple (m,n) over the x and y axes should then present the following reflection phase:

$$\psi^{mn}(f) = -\frac{2\pi f}{c_0}(2r_d)\left[m(sin\theta_r cos\phi_r + sin\theta_i cos\phi_i)\right. \\ \left. -n(sin\theta_r sin\phi_r + sin\theta_i sin\phi_i)\right] + \psi_0, \tag{2}$$

where ψ_0 is the arbitrary phase reference within the AMS (for instance the phase of the central unit-cell). Lastly, besides the disk array presenting the prescribed reflection coefficient phase of Eq.2, the complementary surface is considered as ideally absorbent.

B. Membrane resonator unit-cells

Let's now derive the expression of the reflection coefficient presented by each (passive) circular piston of radius r_d. For the sake of generality, we will denote, in this section, the frequency-dependent acoustic impedance $Z_a(\omega)$ and reflection coefficient $\Gamma(\omega)$ of each vibrating disk, regardless of its position (m,n) within the metasurface. In

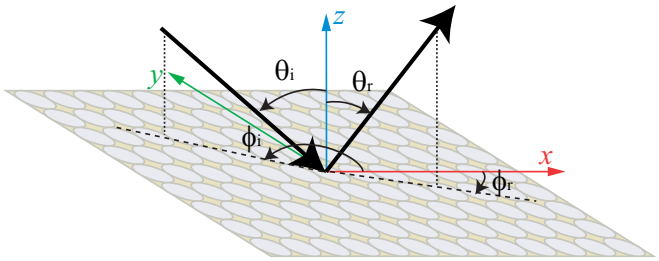

FIG. 1. Definition of the Acoustic Metasurface configuration, and exemple of acoustic wave reflection over the AMS.

the remainder of the paper, we will consider that all unit-cells over the metasurface present the same baseline (passive) acoustic impedance $Z_a(\omega)$, that can be modified by control afterwards. The assignment of a prescribed space- (and frequency-) dependent impedance over the metasurface will be detailed in sec. IV.

In the low-frequency range we may model the small vibrating pistons of Figure 1 as single-degree-of-freedom resonators with mass M_{ms} suspended on their surrounding through an elastic suspension of mechanical compliance C_{ms}, whose losses can be accounted for as a global mechanical resistance R_{ms}. The acoustic impedance[24] of each disk then reads:

$$Z_a(\omega) = j\omega M_{as} + R_{as} + \frac{1}{j\omega C_{as}}, \tag{3}$$

where $M_{as} = \frac{M_{ms}}{S_d}$, $R_{as} = \frac{R_{ms}}{S_d}$, $C_{as} = C_{ms}S_d$ and $S_d = \pi r_d^2$ is the disk area.
The mechanical resonator can also be described by the normalized acoustic resistance r_s, resonance frequency f_s and quality factor Q_s defined as:

$$r_s = \frac{R_{as}}{Z_c}, \tag{4a}$$

$$f_s = \frac{1}{2\pi\sqrt{M_{as}C_{as}}}, \tag{4b}$$

$$Q_s = \frac{1}{R_{as}}\sqrt{\frac{M_{as}}{C_{as}}}, \tag{4c}$$

where $Z_c = \rho_0 c_0$ is the characteristic impedance of the air, and $\rho_0 = 1.2$ kg.m^{-3} the mass density of the air.

The reflection coefficient, under normal incidence, of a resonator of impedance $Z_a(\omega)$ is defined as: $\Gamma(\omega) = \frac{Z_a(\omega)-Z_c}{Z_a(\omega)+Z_c}$. According to Eq.3, it can then be derived as:

$$\begin{aligned}\Gamma(\omega) &= \frac{(R_{as}-Z_c)+j\left(\omega M_{as}-\frac{1}{\omega C_{as}}\right)}{(R_{as}+Z_c)+j\left(\omega M_{as}-\frac{1}{\omega C_{as}}\right)} \\ &= \frac{-\left(\frac{\omega}{\omega_s}\right)^2 + j\left(\frac{\omega}{\omega_s}\right)\frac{1}{Q_s}\left(1-\frac{1}{r_s}\right)+1}{-\left(\frac{\omega}{\omega_s}\right)^2 + j\left(\frac{\omega}{\omega_s}\right)\frac{1}{Q_s}\left(1+\frac{1}{r_s}\right)+1}.\end{aligned} \tag{5}$$

Finally, the reflection phase follows:

$$\begin{aligned}\psi(\omega) &= \tan^{-1}\left(\frac{2Z_c\left(\omega M_{as}-\frac{1}{\omega C_{as}}\right)}{R_{as}^2 - Z_c^2 + \left(\omega M_{as}-\frac{1}{\omega C_{as}}\right)^2}\right) \\ &= \tan^{-1}\left[\frac{2}{r_s Q_s}\frac{\left(\frac{\omega}{\omega_s}\right)^3 - \left(\frac{\omega}{\omega_s}\right)}{\left(\frac{\omega}{\omega_s}\right)^4 + \left(\frac{\omega}{\omega_s}\right)^2\left[\frac{1}{Q_s^2}\left(1-\frac{1}{r_s^2}\right)-2\right]-1}\right].\end{aligned} \tag{6}$$

The inspection of Eq. 6 shows that the proper selection of the mechanical resonator parameters (M_{ms},R_{ms},C_{ms}) (or (r_s,f_s,Q_s)) allows adjusting the reflection phase spanning at any given frequency. However, the achievable phase range over a given frequency bandwidth may vary depending on the resonator characteristics, especially its quality factor and loss factor, namely the value of r_s. In particular, the achievable phase range is limited to less than $[-\frac{\pi}{2},\frac{\pi}{2}]$ for $r_s \geq 1$, which disqualifies such values for spanning the whole unit circle. Therefore, the design of the resonators array is constrained by the selection of Q_s and r_s. In Appendix A, we demonstrate that two important criteria must be considered: first, the mechanical resistance should be chosen so that $r_s < 1$, for example $R_{ms} = \frac{1}{3}S_d Z_c$, in order to allow the reflection phase varying linearly within the broadest frequency band, while spanning a wide range of values within $[0, 2\pi]$; secondly, the resonator quality factor Q_s should neither be too high, since the assumption of linear phase is valid over a limited frequency band only, nor too low since the phase variation may not cover sufficient values within one octave. Therefore, the following mechanical resonator values will be considered in the following:

$$R_{ms} = \frac{Z_c S_d}{3}, \tag{7a}$$

$$Q_s = 6. \tag{7b}$$

The metasurface illustrated in Figure 1 could be theoretically achieved by properly designing discrete passive mechanical resonators presenting the reflection phase grating of Eq. 2 at least over one octave around a desired central frequency f_0. For that, we could tune the resonance frequency of each unit-cell to a given value f^{mn} so that their individual reflection phase at f_0 matches the one targeted on Eq. 2, with the constraints of Eq. 7. However, it is impossible to ensure in practice such variations of mechanical resistance, resonance frequency and quality factor over the whole $M \times N$ unit-cells.

Instead, we propose an active acoustic impedance control strategy to adjust the acoustical properties of the unit-cells along the metasurface. Indeed, it appears to be a more elegant manner than passive construction, potentially allowing for full reconfigurability over a broad bandwidth (at least over one octave). In this paper, the proposed unit-cell concept is realized with a sub-wavelength Active Electroacoustic Resonator (AER) concept. The control principle consists in actively tuning

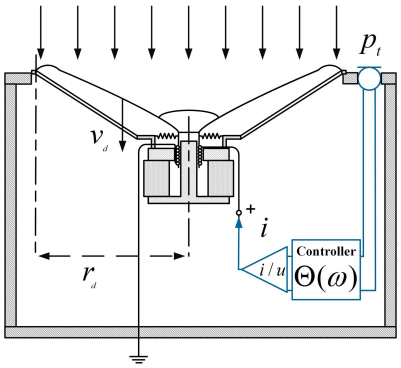

FIG. 2. Description of the AER concept.

the different AER with indices (m, n) to the target resonance frequencies f^{mn}, with a view to shifting their reflection phases $\arg(\Gamma(f_0))$ at f_0 to the prescribed values ψ^{mn}, with a constrained resistance and quality factor. The latter should ensure that the targeted phase grating still holds true over a sufficiently wide frequency band (namely one octave around f_0), assuming a linear phase variation around f_0, according to Appendix A. This means the parameters varied by control should be the passive acoustic mass M_{as} and compliance C_{as} (supposedly the same over the metasurface without control), with a resistance set to $\frac{1}{3}Zc$ for all cells. The following section presents this concept and its application to the acoustic metasurface.

III. ACTIVE ELECTROACOUSTIC UNIT-CELLS

A. Acoustic impedance control principle

Active Electroacoustic Resonators (AER) designate acoustic resonators that can be tuned or modified through electroacoustic control schemes[17–19]. AER can especially be achieved with a control scheme, employing a conventional closed-box electrodynamic loudspeaker diaphragm, the acoustic impedance of which can be controlled through a microphone sensing the total sound pressure p_t in front of the diaphragm, a controller characterized by the transfer function $\Theta(\omega)$ and a transconductance amplifier[19], as illustrated in Figure 2. The volume of free air in the enclosure is denoted V_b, and the loudspeaker diaphragm is assimilated to a single-degree of freedom mechanical resonator with parameters (M_{ms}, R_{ms}, C_{mc}), where C_{mc} accounts both for the free compliance C_{ms} and the additional compliance due to the volume of compressible air V_b inside the enclosure[25]. We can as well define the corresponding acoustic resonator parameters (M_{as}, R_{as}, C_{ac}), as in section II B. Last, the electrodynamic force factor $B\ell$ designates the transduction coefficient of the loudspeaker driver.

If we denote $Z_{as}(\omega) = j\omega M_{as} + R_{as} + \frac{1}{j\omega C_{ac}}$ the "passive" acoustical impedance of the closed-box loudspeaker, $v_d(\omega)$ the diaphragm velocity, and $i(\omega) = \Theta(\omega)p_t(\omega)$ the electrical current circulating through the loudspeaker coil, then the electroacoustic dynamics of the AER can be described in the frequency domain as:

$$Z_{as}(\omega)v_d(\omega) = p_t(\omega)\left(1 - \frac{B\ell}{S_d}\Theta(\omega)\right) \tag{8}$$

The active acoustic impedance Z_a achieved at the loudspeaker diaphragm by the control can be easily derived from Eq. 8 as[19]:

$$Z_a(\omega) = \frac{p_t(\omega)}{v_d(\omega)} = \frac{Z_{as}(\omega)}{1 - \frac{B\ell}{S_d}\Theta(\omega)} \tag{9}$$

Thus, a target frequency-dependent acoustic impedance $Z_{at}(\omega)$ can be chosen, and assigned to the diaphragm if the controller is set to the target transfer function:

$$\Theta_t(\omega) = \frac{S_d}{B\ell}\frac{Z_{at}(\omega) - Z_{as}(\omega)}{Z_{at}(\omega)} \tag{10}$$

B. Target acoustic impedance

Let us now chose the target acoustic impedance $Z_{at}^{mn}(\omega)$ of the (m,n) unit-cell of the AMS as the one of a single-degree of freedom resonator, that eventually differs from the passive loudspeaker diaphragm. For that, we will introduce adjustable coefficients $(\mu_M(m,n), \mu_R(m,n), \mu_C(m,n))$ that will apply to the mass, resistance and compliance of each unit-cell (m,n), so that:

$$Z_{at}^{mn}(\omega) = j\omega\mu_M(m,n)M_{as} + \mu_R(m,n)Z_c + \frac{1}{j\omega\mu_C(m,n)C_{ac}}, \tag{11}$$

where the new resonance frequency of this active acoustic resonator is $f^{mn} = \frac{1}{\sqrt{\mu_M(m,n)\mu_C(m,n)}}f_s$. The controller transfer function should then be set to:

$$\Theta_t^{mn}(\omega) = \frac{S_d}{B\ell}\frac{(j\omega)^2 M_{as}\left(\mu_M(m,n) - 1\right) + j\omega(\mu_R(m,n)Z_c - R_{as}) + \left(\frac{1-\mu_C(m,n)}{\mu_C(m,n)C_{ac}}\right)}{(j\omega)^2\mu_M(m,n)M_{as} + j\omega\mu_R(m,n)Z_c + \frac{1}{\mu_C(m,n)C_{ac}}} \tag{12}$$

The control principle introduced at the end of Section II B then consists in identifying the coefficient pair $\mu_M(m,n)$ and $\mu_C(m,n)$ ($\mu_R(m,n)$ being fixed to 1/3) for each unit-cell (m,n) of the AMS, allowing shifting the resonance frequency from f_s to a target (active) resonance frequency f^{mn}, defined in the next section. The next section introduces a methodology for setting these coefficients, with the aim of achieving desired anomalous reflection angle (ϕ_r,θ_r) for a given incidence (ϕ_i,θ_i), over at least one octave around a given central frequency f_0.

IV. ACTIVE ACOUSTIC METASURFACE

A. Parametrization of the Active Unit-Cells

We will consider an AMS consisting of an array of $M \times N$ small commercially-available electrodynamic loudspeaker (Monacor SPX-30M, whose Thiele-Small parameters of which are given in Table I). Their radius $r_d \approx 32$ mm limits the frequency range of operation as metasurface unit-cells to $f_{max} = 500$ Hz. Moreover, we will consider $\phi_r = \phi_i = 0\,(\mod \pi)$, yielding an impedance grating only over the x dimension. Under this assumption, the space-dependence along y collapses, and the acoustic impedance of each AER within a same row m will be controlled to achieve the target reflection phase:

$$\psi^m(f_0) = -\frac{2\pi f_0}{c_0}(2r_d)m(sin\theta_r + sin\theta_i) + \psi_0 \quad (13)$$

The following presents a simple methodology to assign a target reflection angle θ_r for a given incident angle θ_i, at a given central frequency f_0, with a metasurface of lattice constant $2r_d$. By using the control law of Eq. 12 , the acoustic impedance of each unit-cell m over the metasurface will be simply shifted in frequency so that the reflection phase at f_0 matches a target value $\psi^m(f_0)$, following Eq. 13.
We also impose the phase of the $(\mathrm{M}/2{+}1)^{\mathrm{th}}$ cell $\psi^{M/2+1}(f_0) = -\pi$, so that the whole metasurface phases may vary within [-2π; 0]. Under these conditions, there exists only one frequency f^m for which the phase of the reflection coefficient of the $(\mathrm{M}/2{+}1)^{\mathrm{th}}$ cell matches the target value ψ^m: $\arg(\Gamma^{M/2+1}(f^m)) = \psi^m\,(\mod 2\pi)$.
Figure 3, represents the reflection phase $\arg(\Gamma^{\mathrm{M}/2+1}(f))$ analytically computed in Matlab with Eq.6, corresponding to the acoustic impedance of the $(\mathrm{M}/2{+}1)^{\mathrm{th}}$ cell $Z_{at}^{\mathrm{M}/2+1}(\omega)$ defined in Eq.11, with $\mu_M(\mathrm{M}/2{+}1) = \mu_C(\mathrm{M}/2{+}1) = 1$ and $\mu_R(\mathrm{M}/2{+}1) = 1/3$. The different values of ψ^m drawn as round markers on Figure 3 are defined for an array size $M = 32$, for the reflection case $\theta_i = -\frac{\pi}{4}$ and $\theta_r = \frac{\pi}{3}$. Assuming a linear phase variation of the reflection coefficient Γ around f_0, the target reflection phase $\arg(\Gamma^m(f_0))$ can be achieved at f_0 on cell m by shifting the resonance frequency of the m^{th} active

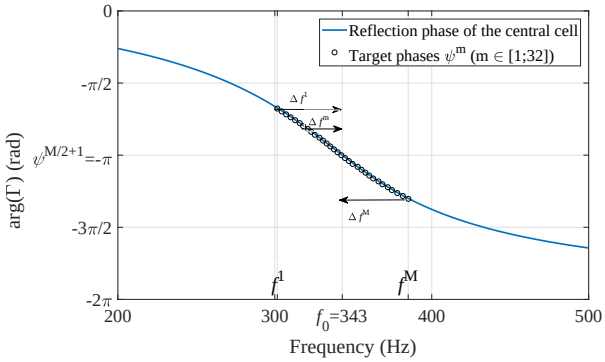

FIG. 3. Reflection phase to prescribe to the 17^{th} cell within a metasurface with M=32 rows, computed for the case ($\theta_i = -\frac{\pi}{4}$,$\theta_r = \frac{\pi}{3}$), imposing a quality factor Q_s=16 and resistance factor $\mu_R = 1/3$ (blue line). Identification of the target reflection phases (round markers) and corresponding resonance shifts $\Delta f^m = f_0 - f^m$.

AER by a value $\Delta f^m = f_0 - f^m$. This is finally done by assigning:

$$\mu_M(m).\mu_C(m) = \left(\frac{f_0}{f^m}\right)^2, \quad (14)$$

while preserving the resonance quality factor $Q_s = 6$ and resistance $R_{as} = \frac{1}{3}Z_c$, as explained in Appendix A. Finally, the coefficients can be identified as:

$$\mu_R(m) = \frac{1}{3} \quad (15a)$$

$$\mu_C(m) = \frac{1}{2\pi Z_c C_{ac} Q_s}\frac{1}{(f_0 + \Delta f^m)\mu_R(m)} \quad (15b)$$

$$\mu_M(m) = \frac{Z_c Q_s}{2\pi M_{as}}\frac{\mu_R(m)}{(f_0 + \Delta f^m)} \quad (15c)$$

Then, the impedance of each cell within row m is assigned thanks to the individual control law $\Theta_t^m(\omega)$, as in Eq. 12. The methodology for designing the AMS can then be summarized as follows:

1. choice of the target reflected angle θ_r for a given incident angle θ_i (at frequency f_0);
2. definition of the reflection phase grating ψ^m over the metasurface of lattice constant $2r_d$ according to Eq.13;
3. definition of the reflection phase reference at the $(\mathrm{M}/2{+}1)^{\mathrm{th}}$ cell such as $\arg(\Gamma^{\mathrm{M}/2+1}(f_0)) = -\pi$;
4. identification of the resonance shift $\Delta f^m = f_0 - f^m$ for each cell over the metasurface, so that $\arg(\Gamma^{\mathrm{M}/2+1}(f^m)) = \psi^m$;
5. identification of the control parameters $\mu_M(m)$, $\mu_C(m)$ and μ_R achieving such resonance shift (Eq. 15);
6. modification of the acoustic impedance of the m^{th} cell with the controller $\Theta_t^m(\omega)$ of Eq.12.

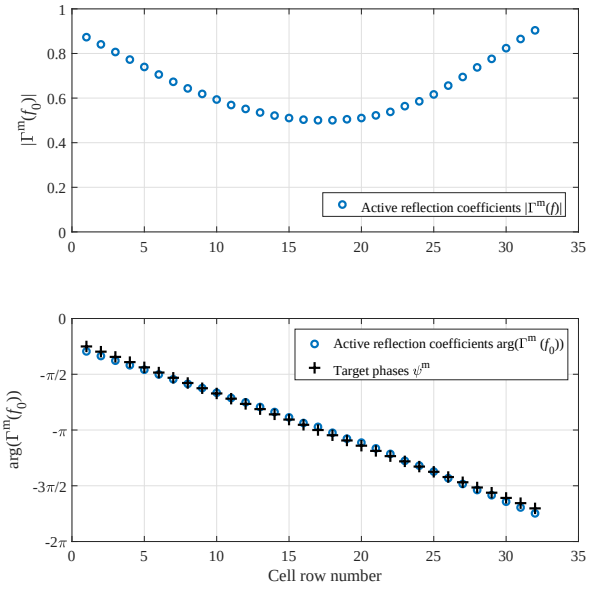

FIG. 4. Blue circles: Achieved reflection coefficients at $f_0 =$ 343 Hz with M=32 rows (top: amplitude; bottom: phases). Comparison to the targeted values ψ^m (black dotted line).

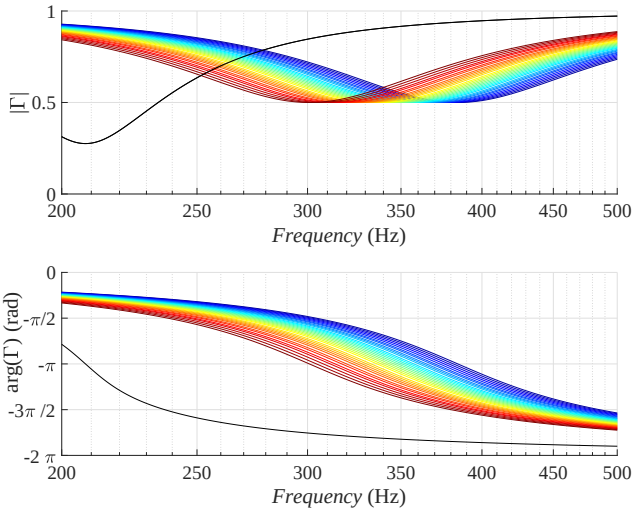

FIG. 5. Rainbow-coloured lines: target reflection coefficients of the 32 unit-cells (from cell #1 in blue to cell #32 in red) of the metasurface, for $\theta_i = -\pi/4$ and $\theta_r = \pi/3$ (top: amplitude, bottom: phase), computed in Matlab with Eq.5. Comparison to the reflection coefficient of the passive Electroacoustic Resonator (black lines).

Figure 4 shows an example of the reflection coefficient targeted at f_0 =343 Hz on each cell m for an array size $M = 32$, for the reflection case ($\theta_i = -\frac{\pi}{4}$,$\theta_r = \frac{\pi}{3}$). Figure 5 presents the bode diagrams of the 32 reflection coefficients $\Gamma^m(\omega)$ that can be achieved on the 32 cells of the AMS, analytically computed in Matlab from Eq. 5, with the target impedances $Z^m_{at}(\omega)$ defined in Eq.11.

B. Experimental Assessment of the Unit-Cells

The target reflection coefficients have been programmed on a unit-cell prototype, consisting of a MONACOR SPX-30M loudspeaker in a small wooden enclosure. The Thiele-Small parameters[25] of the closed-box loudspeaker are estimated, following the methodology proposed by Seifel et al.[26], in an impedance tube from two measurements of the acoustic impedance at the diaphragm, first with the loudspeaker terminals in open circuit, and then in short circuit (more details are provided in Ref.[27], pp. 50-52). The loudspeaker diaphragm is excited by an exogenous sound source located at the other end of the duct with broadband noise. The acoustic radiation impedance of the loudspeaker under test, which depends on the environment in which it is located, has been taken into account in the acoustic impedance Z_{as} to avoid numerous annotations. These parameters are presented in Table I.

The reflection coefficient of the unit-cell prototype diaphragm, mounted in a custom-made impedance tube, is assessed according to the two-microphones methods described in ISO 10534-2 standard[28]. The transfer functions H_{12} between microphones 1 and 2 positions along the tube are processed through a Multichannel Analyzer (Bruel & Kjaer Pulse Type 3160), and the reflection coefficient of the diaphragm can be derived.

On the Active Electroacoustic Resonator side, the total pressure p_t used in the control is sensed with a PCB 130D20 microphone, located at 5 mm from the electroacoustic absorber membrane and close to the lateral duct wall of the impedance tube as depicted in Fig. 6. Each transfer function $\Theta^{mn}_t(\omega)$ given by Eq.(12) and (15) applied to the corresponding cell is discretized into an infinite impulse response filter using the Tustin method, then is implemented onto a real-time National Instruments CompactRIO platform supporting field-programmable gate array (FPGA) technology. The voltage signal from the microphone is then digitally converted at a sampling frequency of 80 kHz thanks to an analog module NI 9215, and the output filtered signal u_{out} is delivered by an

TABLE I. Measured Thiele-Small parameters of the MONACOR SPX-30M loudspeaker.

Parameter	Symblol	Value	Unit
Effective piston area	S_d	32	cm^2
Mechanical mass	M_{ms}	3.17	g
Mechanical resistance	R_{ms}	0.75	$N.s.m^{-1}$
Mechanical compliance (with enclosure)	C_{mc}	184.10^{-6}	$m.N^{-1}$
Force factor	$B\ell$	3.67	N/A
Resonance frequency	f_s	208	Hz
Quality factor	Q_s	5.5	

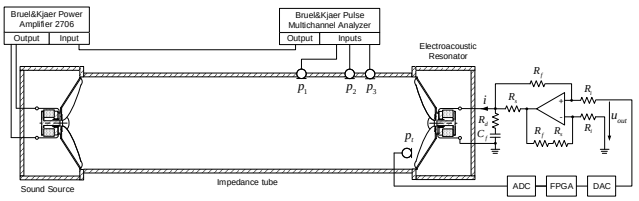

FIG. 6. Scheme of the experimental setup. The control implementation is depicted in the right-hand side including the microphone, the digital controller and the transconductance amplifier.

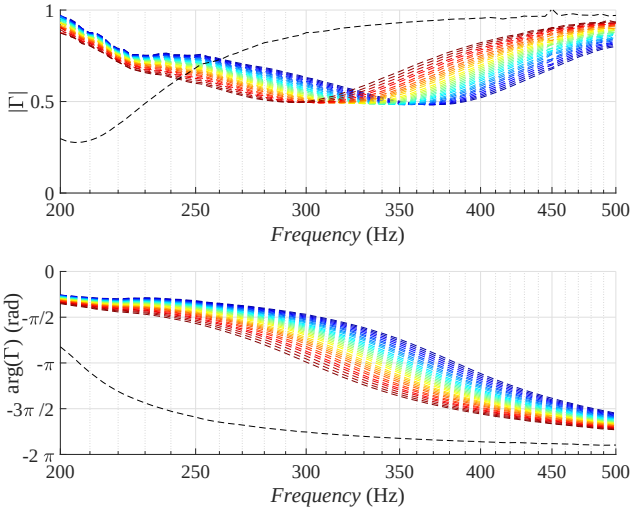

FIG. 7. Rainbow-coloured dotted lines: measured achieved reflection coefficient (top: amplitude, bottom: phase) of the 32 unit-cells (from cell #1 in blue to cell #32 in red) of the metasurface, for $\theta_i = -\pi/4$ and $\theta_r = \pi/3$). Comparison to the reflection coefficient measured on the passive Electroacoustic Resonator (black dotted lines).

analog module NI 9263. The overall time delay of the controller (ADC/FPGA/DAC) is equal to 20.6 μs. A voltage controlled current source, involving an op-amp based improved Howland current pump circuit as illustrated in Fig.6, has to be implemented downstream the digital controller, so that to properly drive the voice-coil loudspeaker in current. The details of the digital controller implementation can be found in Ref.[19] and Ref.[27] (pp. 57-58), and more information about the stability and control limitations of the acoustic impedance control can be found in Ref.[27] (pp. 73-81).

Figure 7 shows the reflection coefficients measured on the unit-cell prototype, for each of the 32 control settings. The results are compared to the passive reflection coefficient of the unit-cell. We can see that the targeted reflection coefficients are actually achieved with the proposed unit-cell and control framework. Moreover, it is noticeable in this example that the passive resonance frequency is one octave lower than the highest active resonance frequency of the 32 unit-cells, which shows the range of tunability of the control framework.

V. RESULTS AND DISCUSSION

Once the target reflection coefficients have been verified experimentally, the metasurface is numerically modelled on a commercial Finite-Elements Software (COMSOL Multiphysics 5.3). The full-wave simulation is performed with the Pressure Acoustic (Frequency Domain) physics, considering periodic conditions over the y axis, thus limiting the metasurface to a single line of $M = 32$ circular disks of radius r_d, regularly dispatched along the x axis (with lattice constant $2r_d$). The considered propagating domain is then a half-cylinder (symmetry axis along y) of radius $L = 6$ m (including a Perfectly Matched Layer), and height $2r_d$ (to ensure the same lattice constant over y). Each lateral sides of the cylinder are assigned "Sound Hard Boundary" conditions. Each disk representing an AER on the xy plane is assigned an acoustic impedance boundary condition, which is defined as in Eq.11 considering the control parameters of Eq.15, and the remaining area on the xy plane is considered perfectly absorbent (impedance matching condition). We also consider a tetrahedral meshing inside the propagating domain, with mesh size corresponding to 6 nodes per wavelength at 450 Hz. A refinement of the mesh is also processed at the level of the metasurface elements, with an additional triangular meshing (refinement by a factor 10 along x and y axes).

The "Background Pressure Field" is finally employed to impose an incident plane wave with wave vector $(\cos(\theta_i), 0, \sin(\theta_i))$ and amplitude 1 Pa. In this paper, we will consider the incident plane wave fields impinges the metasurface with incident angle $\theta_i = -\frac{\pi}{4}$ rad, and two reflection cases:

- $\theta_r = \frac{\pi}{3}$ rad, corresponding to an augmentation of the reflected angle,
- $\theta_r = 0$ rad, corresponding to a diminution of the reflected angle.

Figures 8 and 9 represent the reflected sound pressure levels maps over the xz plane, processed by full-wave simulations, for the two studied cases, at f =350 Hz. It can be seen that the acoustic impedance imposed on the metasurface unit-cells actually allows steering the wavefronts toward the prescribed angle. Since the reflection coefficient amplitude of the whole metasurface unit-cells range between 0.5 and 0.6 at f_0 (as can be seen for example on Figure 4), an expected attenuation of the reflected energy is observed.

Figures 10 and 11 present the directivity of the metasurface, namely a polar representation of the normalized sound pressure levels (referred to the maximal value), processed by full-wave simulations at a distance r =3 m from the metasurface center, for both reflection cases

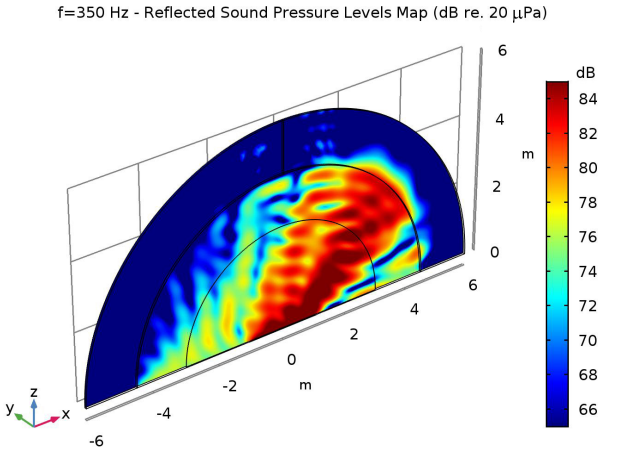

FIG. 8. Reflected sound pressure levels (dB re. 20 μPa) obtained by full-wave simulations with 32x32 unit-cells, at $f = 350$ Hz, for $\theta_i = -\frac{\pi}{4}$ rad. and $\theta_r = \frac{\pi}{3}$ rad.

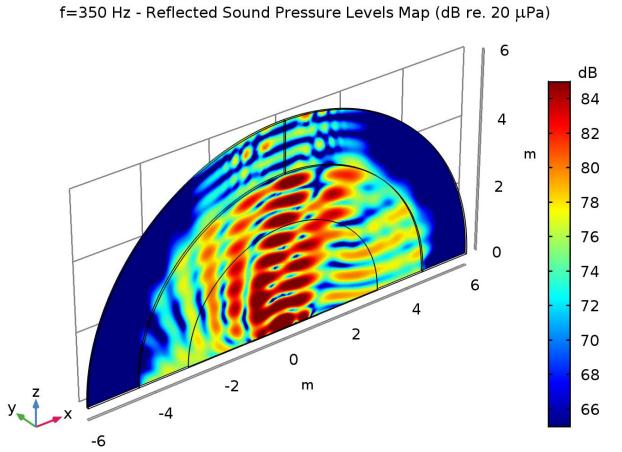

FIG. 9. Reflected sound pressure levels (dB re. 20 μPa) obtained by full-wave simulations with 32x32 unit-cells, at $f = 350$ Hz, for $\theta_i = -\frac{\pi}{4}$ rad. and $\theta_r = 0$ rad.

($\theta_r = \frac{\pi}{3}$ rad, and $\theta_r = 0$ rad) and at different frequencies (200 Hz - 250 Hz - 350 Hz and 400 Hz). First, the limited size of the AMS (2 meters long) with respect to the studied wavelength explains the occurrence of side lobes. We can also observe that the beam widths depend on frequency. Finally, it seems that the beam shapes are much more spread over angles for the case $\theta_r = \frac{\pi}{3}$ rad than the case $\theta_r = 0$ rad, which can be explained by the fact that the 32 cells span a smaller range of reflection phases over $[-2\pi - 0]$ in the first case. This could be alleviated by designing an AMS with a higher number of unit-cells. But in general, there is a good agreement between the achieved directivities and the targeted reflected angles, which confirm the effectiveness of the AER to achieve a coherent steering over a relatively wide frequency band (almost one octave around 350 Hz).

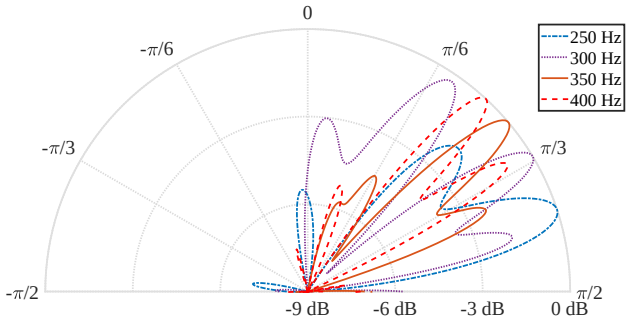

FIG. 10. Reflection directivities (polar representation of reflected sound pressure levels in dB referred to the maximal value) obtained by full-wave simulations with 32x32 unit-cells, at frequencies $f = \{250, 300, 350, 400\}$ Hz, for $\theta_i = -\frac{\pi}{4}$ rad. and $\theta_r = \frac{\pi}{3}$ rad.

VI. CONCLUSIONS

We have proposed Active Electroacoustic Resonators as unit-cells within an acoustic metasurface, in a reflectarray application. The reflection properties have been derived to define individual control laws to assign to each AER unit-cells. The identified control settings have been applied to a conventional electrodynamic loudspeaker in a view to assessing the feasibility of the targeted reflection phases along a metasurface of 32 elements. Then Full-Wave simulations have been processed to simulate the achieved reflection properties with the targeted control settings, showing the effectiveness of the concept for steering wavefronts in a prescribed manner. Moreover, we have shown the effectiveness of the control over a relatively wide frequency band, opening the way to actual applications as reflectarray for audible sounds. Further developments should focus on designing an actual proto-

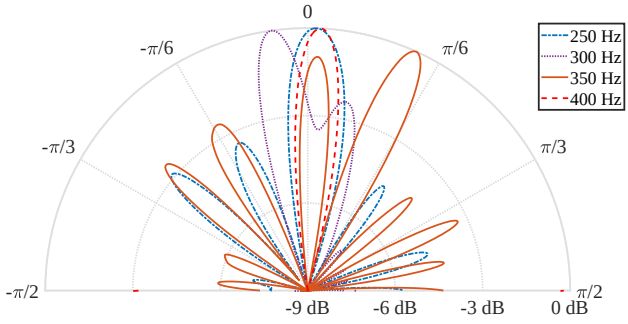

FIG. 11. Reflection directivities (polar representation of reflected sound pressure levels in dB referred to the maximal value) obtained by full-wave simulations with 32x32 unit-cells, at frequencies $f = \{250, 300, 350, 400\}$ Hz, for $\theta_i = -\frac{\pi}{4}$ rad. and $\theta_r = 0$ rad.

type of metasurface with a hardware allowing individually controlling 32 unit-cells. It is likely to demonstrate the actual performance of the concept, owing to a ad hoc experimental setup to be developed.

The proposed methodology for controlling the reflection coefficient phase over the metasurface is based on the assumption of a linear phase variation, over a large bandwidth around the central frequency f_c. This simplistic assumption is somehow limiting, both in terms of achievable reflection phases than in terms of accurate phase grating over the surface. Other methodologies based on more complex acoustic impedance control strategies, such as Active Multiple-Degrees-Of-Freedom Electroacoustic Resonators, coupled with an optimization procedure as proposed in Ref.[20], could also help improving the concept.

ACKNOWLEDGMENTS

The authors wish to thank Hussein Esfahlani for the advices on the design of the acoustic metasurface in the COMSOL Multiphysics environment.

Appendix A: Discussion on the choice of a passive resonator

We consider a single-degree of freedom resonator (r,m,c), the normalized impedance of which reads $z = \frac{Z_a}{Z_c} = j\omega m + r + \frac{1}{j\omega c}$. We also define its resonance frequency $\omega_s = \sqrt{mc}^{-1}$ and quality factor $Q_s = (\omega_s r c)^{-1}$. The reflection coefficient $\Gamma(\omega)$ then reads:

$$\Gamma(\omega) = \frac{\left[1 - \left(\frac{\omega}{\omega_s}\right)^2\right] + j\left(\frac{\omega}{\omega_s}\right) Q_s^{-1}(1 - r^{-1})}{\left[1 - \left(\frac{\omega}{\omega_s}\right)^2\right] + j\left(\frac{\omega}{\omega_s}\right) Q_s^{-1}(1 + r^{-1})} \quad \text{(A1)}$$

We first vary the values of the resistance r with a fixed quality factor $Q_s = 1$. The bode diagram of the reflection coefficient is presented in Figure 12. The inspection of the reflection coefficient shows that, for a unitary resonance quality factor, when $r < 1$, the reflection coefficient spans the whole 2π, whereas values of $r > 1$ yield smaller ranges of the reflection coefficient phase. Therefore, the necessity to achieve reflection phases spanning the whole $[0 - 2\pi]$ range motivates the choice of an acoustic resistance lower than Z_c. It is also noticeable that, for values $r \approx 1/3$, the reflection coefficient phase variation varies linearly with frequency on the broadest frequency band. Moreover, since the minimal reflection coefficient value for $r = 1/3$ is $\Gamma = 0.5$, it might be timely to chose values of resistances varying around this value for the whole unit-cells.

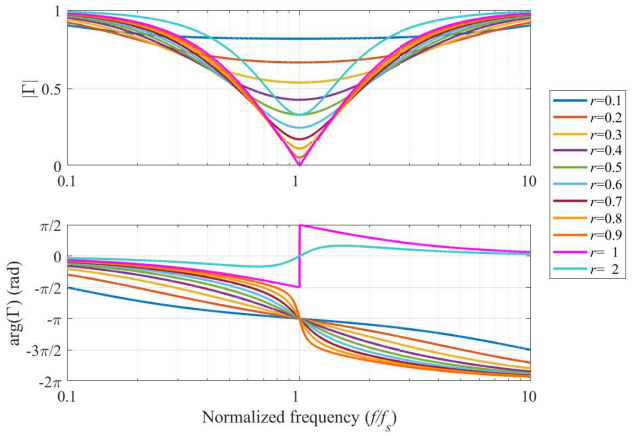

FIG. 12. Bode diagram of the reflection coefficient of a SDOF resonator, with constant quality factor Q_s=1 and varying resistances ($r \in [0.1, 10]$)

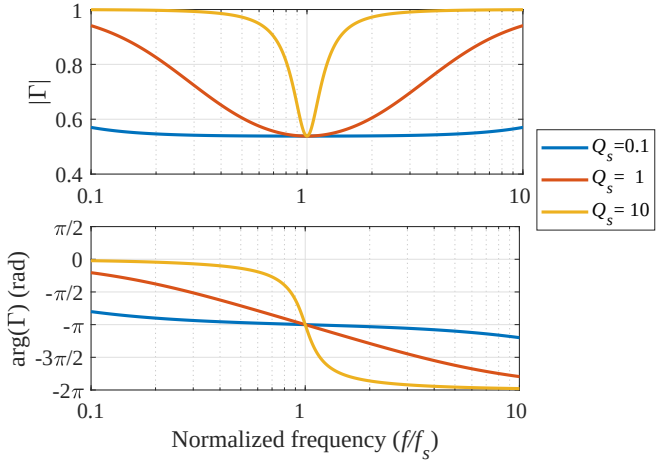

FIG. 13. Bode diagram of the reflection coefficient of a SDOF resonator, with constant resistance r=0.3 and varying quality factors ($Q \in [0.1, 10]$)

Then, if we set the resistance $r = 0.3$, we can assess the sensitivity of the reflection phase variation to the quality factor, as illustrated in Figure 13. For a low value of Q_s, the reflection phase does not span a sufficiently wide range. For a high value of Q_s, the phase variation is linear only over a too narrow frequency band (an objective limit could be one octave). There is then a compromise to find between the different phase profiles (eg. spanning over the whole trigonometric circle vs. bandwidth extension). Then, we have chosen to set $r = 0.3$ and $Q_s = 6$ to allow a wide range of reflection coefficient control over at least one octave.

[1] S. A. Cummer, J. Christensen, and A. Alù, "Controlling sound with acoustic metamaterials," Nature Reviews Materials **1**, 16001 (2016).
[2] H. Esfahlani, S. Karkar, H. Lissek, and J. R. Mosig, "Acoustic dispersive prism," Scientific reports **6**, 18911 (2016).

[3]H. Esfahlani, S. Karkar, H. Lissek, and J. R. Mosig, "Exploiting the leaky-wave properties of transmission-line metamaterials for single-microphone direction finding," The Journal of the Acoustical Society of America **139**, 3259–3266 (2016).

[4]H. Esfahlani, S. Karkar, H. Lissek, and J. R. Mosig, "Acoustic carpet cloak based on an ultrathin metasurface," Physical Review B **94**, 014302 (2016).

[5]X. Wang, D. Mao, and Y. Li, "Broadband acoustic skin cloak based on spiral metasurfaces," Scientific Reports **7** (2017).

[6]H. Esfahlani, H. Lissek, and J. R. Mosig, "Generation of acoustic helical wavefronts using metasurfaces," Physical Review B **95**, 024312 (2017).

[7]A. B. Khanikaev, R. Fleury, S. H. Mousavi, and A. Alù, "Topologically robust sound propagation in an angular-momentum-biased graphene-like resonator lattice," Nature communications **6** (2015).

[8]S. Yves, R. Fleury, F. Lemoult, M. Fink, and G. Lerosey, "Topological acoustic polaritons: robust sound manipulation at the subwavelength scale," New Journal of Physics **19**, 075003 (2017).

[9]Y. Li and B. M. Assouar, "Acoustic metasurface-based perfect absorber with deep subwavelength thickness," Applied Physics Letters **108**, 063502 (2016).

[10]Y. Li, B. Liang, Z.-m. Gu, X.-y. Zou, and J.-c. Cheng, "Reflected wavefront manipulation based on ultrathin planar acoustic metasurfaces," Scientific reports **3**, 2546 (2013).

[11]C. Faure, O. Richoux, S. Félix, and V. Pagneux, "Experiments on metasurface carpet cloaking for audible acoustics," Applied Physics Letters **108**, 064103 (2016).

[12]N. Jiménez, T. J. Cox, V. Romero-García, and J.-P. Groby, "Metadiffusers: Deep-subwavelength sound diffusers," Scientific Reports **7** (2017).

[13]S. Lani, K. G. Sabra, and F. L. Degertekin, "Modal and transient analysis of membrane acoustic metasurfaces," Journal of Applied Physics **117**, 045308 (2015), https://doi.org/10.1063/1.4906549.

[14]L. D. Landau, J. Bell, M. Kearsley, L. Pitaevskii, E. Lifshitz, and J. Sykes, *Electrodynamics of continuous media*, Vol. 8 (elsevier, 2013).

[15]B.-I. Popa, D. Shinde, A. Konneker, and S. A. Cummer, "Active acoustic metamaterials reconfigurable in real time," Phys. Rev. B **91**, 220303 (2015).

[16]X. Chen, P. Liu, Z. Hou, and Y. Pei, "Magnetic-control multifunctional acoustic metasurface for reflected wave manipulation at deep subwavelength scale," Scientific Reports **7** (2017).

[17]H. Lissek, R. Boulandet, and R. Fleury, "Electroacoustic absorbers: bridging the gap between shunt loudspeakers and active sound absorption," The Journal of the Acoustical Society of America **129**, 2968–2978 (2011).

[18]R. Boulandet, E. Rivet, and H. Lissek, "Sensorless electroacoustic absorbers through synthesized impedance control for damping low-frequency modes in cavities," Acta Acustica united with Acustica **102**, 696–704 (2016).

[19]E. Rivet, S. Karkar, and H. Lissek, "Broadband low-frequency electroacoustic absorbers through hybrid sensor-/shunt-based impedance control," IEEE Transactions on Control Systems Technology **25**, 63–72 (2017).

[20]E. Rivet, S. Karkar, and H. Lissek, "On the optimisation of multi-degree-of-freedom acoustic impedances of low-frequency electroacoustic absorbers for room modal equalisation," (2017), (in Production) in Acta Acustica united with Acustica.

[21]R. Fleury, D. L. Sounas, and A. Alù, "Negative refraction and planar focusing based on parity-time symmetric metasurfaces," Phys. Rev. Lett. **113**, 023903 (2014).

[22]R. Fleury, D. Sounas, and A. Alù, "An invisible acoustic sensor based on parity-time symmetry," Nature communications **6**, 5905 (2015).

[23]R. Fleury, D. L. Sounas, and A. Al, "Parity-time symmetry in acoustics: Theory, devices, and potential applications," IEEE Journal of Selected Topics in Quantum Electronics **22**, 121–129 (2016).

[24]Here we define the acoustic impedance as a ratio between sound pressure and particle velocity, although it is conventionally defined as the ratio between pressure and flow velocity[25].

[25]M. Rossi, "Audio," (Presses Polytechniques Fédérales de Lausanne, 2007) Section 9.1, pp. 533–540.

[26]U. Seidel and w. Klippel, "Fast and accurate measurement of the linear transducer parameters," in *Audio Engineering Society Convention 110* (2001).

[27]E. Rivet, *Room Modal Equalisation with Electroacoustic Absorbers*, Ph.D. thesis, Ecole Polytechnique Fédérale de Lausanne (2016), (accessible on https://infoscience.epfl.ch/record/222866).

[28]"Iso 10534-2-1998 : Acoustics - determination of sound absorption coefficient and impedance in impedance tubes - part 2 : Transfer-function method," ISO, Geneva, Switzerland (1998).